

# Fibro-Gel: An All-Aqueous Hydrogel Consisting of Microfibers with Tunable Release Profile and its Application in Wound Healing

Yanting Shen, Yuan Liu, Janine K. Nunes, Chenmin Wang, Miao Xu, Michael K.T. To,\* Howard A. Stone,\* and Ho Cheung Shum\*

Injectable hydrogels are valuable tools in tissue engineering and regenerative medicine due to their unique advantages of injectability with minimal invasiveness and usability for irregularly shaped sites. However, it remains challenging to achieve scalable manufacturing together with matching physicochemical properties and on-demand drug release for a high level of control over biophysical and biomedical cues to direct endogenous cells. Here, the use of an injectable fibro-gel is demonstrated, a water-filled network of entangled hydrogel microfibers, whose physicochemical properties and drug release profiles can be tailored to overcome these shortcomings. This fibrogel exhibits favorable in vitro biocompatibility and the capability to aid vascularization. The potential use of the fibro-gel for advancing tissue regeneration is explored with a mice excision skin model. Preliminary in vivo tests indicate that the fibro-gel promotes wound healing and new healthy tissue regeneration at a faster rate than a commercial gel. Moreover, it is demonstrated that the release of distinct drugs at different rates can further accelerate wound healing with higher efficiency, by using a two-layer fibro-gel model. The combination of injectability and tailorable properties of this fibro-gel offers a promising approach in biomedical fields such as therapeutic delivery, medical dressings, and 3D tissue scaffolds for tissue engineering.

Y. Shen, Y. Liu, M. Xu, H. C. Shum
Department of Mechanical Engineering
The University of Hong Kong
Pokfulam Road, Hong Kong SAR, China
E-mail: ashum@hku.hk
J. K. Nunes, H. A. Stone
Department of Mechanical and Aerospace Engineering
Princeton University
Princeton, NJ 08544, USA
E-mail: hastone@princeton.edu
C. Wang, M. K.T. To
Department of Orthopaedics and Traumatology
LKS Faculty of Medicine

Department of Orthopaedics and Traumatology LKS Faculty of Medicine University of Hong Kong Pokfulam Road, Hong Kong SAR, China E-mail: mikektto@hku.hk

The ORCID identification number(s) for the author(s) of this article can be found under https://doi.org/10.1002/adma.202211637.

© 2023 The Authors. Advanced Materials published by Wiley-VCH GmbH. This is an open access article under the terms of the Creative Commons Attribution License, which permits use, distribution and reproduction in any medium, provided the original work is properly cited.

DOI: 10.1002/adma.202211637

### 1. Introduction

Hydrogels have various biomedical applications such as tissue-engineered constructs,<sup>[1]</sup> drug delivery systems,<sup>[2]</sup> cellbased therapies, [3] wound dressings, [2b,4] and antiadhesion materials.<sup>[5]</sup> The use of hydrogels is a consequence of their being composed of a large amount of water and a crosslinked polymer network that provides physical similarity to the extracellular matrix and the capability to easily encapsulate drugs.<sup>[6]</sup> Cell and cytokine therapeutics can be significantly enhanced via encapsulation within hydrogels,[7] due to stabilization during delivery,[2b,8] protection from the immune system in vivo, [9] and localization to the intended delivery region, [10] ultimately extending the therapeutic window.

Recently, the evolution of injectable hydrogels has been driven by the need to overcome the drawback of the pre-formed hydrogel for recapitulating natural tissue function with a minimally invasive implantation procedure. <sup>[3b,11]</sup> The injectable hydro-

gels not only have the typical advantages of conventional hydrogels but they can also be injected with minimal invasiveness into target sites and used for irregularly shaped sites. Accordingly, they have been developed as a promising and successful material system for many biomedical applications including the delivery of therapeutic agents for the treatment of infectious diseases<sup>[2a]</sup> and for the regeneration of tissues such as bone, cartilage, muscle, and skin.<sup>[12]</sup>

However, there still are several major challenges to enhancing care with hydrogels and reducing costs and waste: i) Poorly scalable fabrication of a functional hydrogel hinders the wider clinical applications and wastes resources. [13] A simple and cost-effective manufacturing system with high throughput would provide a much-needed boost to enable the utility of functional hydrogels in a variety of industrial settings. ii) It is difficult using the existing hydrogels to precisely tailor mechanical properties for individual cases to match specific cell regeneration requirements. The mechanical properties of hydrogels affect the fate and phenotype of the extracellular matrix. [14] For instance, the elastic moduli of 0.1–1 kPa influence mesenchymal stem cell differentiation. [14] iii) Controlling the release of distinct molecules at different rates from existing hydrogels remains a challenge. The potential importance of tunable drug release rates is exemplified

ADVANCED MATERIALS

www.advmat.de

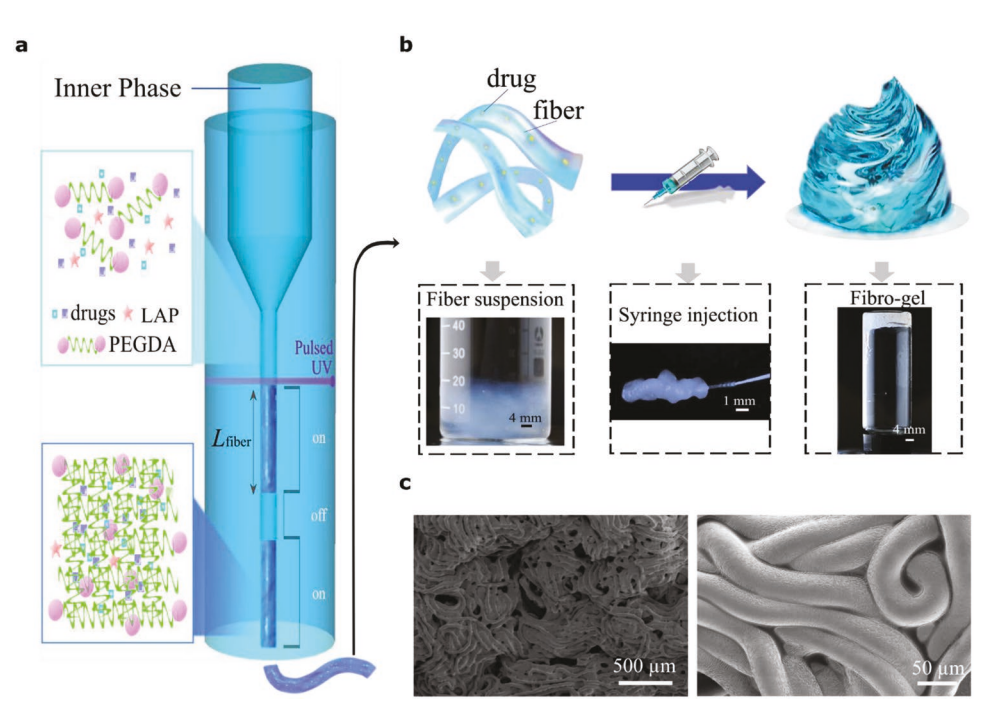


**Figure 1.** Fabrication of fibro-gel. a) Schematic illustrations of the microfiber generation using a co-flow microfluidic device. The inner phase contains polymer (PEGDA), photoinitiator (LAP), and drug (TC/EGF). The drug-loaded microfibers are synthesized by pulsed UV illumination. The flow rates are fixed and the length of the fiber,  $L_{\text{fiber}}$ , is adjusted by the exposure time. b) Extrusion of the fibro-gel from a needle, where the fibro-gel is formed from a suspension of fibers. The extruded fibro-gel is viscoelastic with a high viscosity. c) SEM image of a dried fibro-gel, with a magnified image (right) showing the micromorphology of the fibro-gel.

by the fact that tissue repair and regeneration involve the sequential signaling of several growth factors.<sup>[2a]</sup> Therefore, controllable hydrogel dressings with the ability to provide customized treatment settings and modify drug release profiles at different rates for diverse tissue engineering applications are urgently needed.

Here, we develop an injectable fibro-gel with controllable physicochemical properties and drug release rates by changing the length of the individual fibers that make up the gel. The fibro-gel refers to a gel that is formed upon extrusion of a suspension of long, flexible microfibers.[15] Based on this flowinduced gelation mechanism, we sought to synthesize an oilfree, biocompatible, biomimetic, and fully scalable hydrogel material with a wide range of properties for use. Benefiting from tetracycline (TC) and epidermal growth factor (EGF) loaded inside the microfiber, as shown in Figure 1a, the fibro-gel exhibited biological active functions: antibacterial activity and vascularization, which were verified with both in vitro and in vivo experiments. In addition, we explored the potential of fibro-gel for clinical applications by using an excisional wound healing model. In vivo, the drug-loaded fibro-gel served as a wound dressing demonstrating significantly improved therapeutic outcomes compared to a commercial gel (Hydrosorb Gel).

# 2. Results and Discussion

# 2.1. From Microfiber Suspension to Fibro-Gel

For the fabrication of the fibro-gel, instead of traditional oil/aqueous systems, [15] we used the aqueous two-phase system

(ATPS), [16] poly(ethylene glycol) diacrylate (PEGDA) and potassium phosphate tribasic, to fabricate the microfibers using continuous flow microfluidic methods. After reaching phase equilibria, the polymer-rich phase was mixed with a photoinitiator, lithium phenyl-2,4,6-trimethylbenzoylphosphinate (LAP), and drugs, e.g., tetracycline (TC) and/or epidermal growth factor (EGF), and then flowed as the inner phase. The salt-rich phase was used as the outer phase for forming the co-flow configuration. The flow rates of the outer and inner phases were fixed during the whole fabrication procedure, which created a uniform inner flow with a central stream of diameter 110 µm. Pulsed UV illumination was used to segment a continuous pre-gel aqueous phase into uniform microfibers, as shown in Figure 1a. The length of the fiber,  $L_{\text{fiber}}$  is proportional to the product of the flow rate and the exposure time (the "pulse on" time). In our study,  $L_{\mathrm{fiber}}$  was only adjusted by the UV exposure time due to the fixed flow rates.

After collecting a certain volume of microfibers from the microfluidic device, the injection strategy was adapted to form the fibro-gel from the microfiber suspensions, as shown in Figure 1c and Movie S1, Supporting Information. Triggered by a flow-induced mechanism that produced physical entanglements, <sup>[15]</sup> upon extrusion the fiber suspension was converted into a viscoelastic gel, with no additional chemical reactions or post-processing required. This approach can be extended to fabricate fibers using most photosensitive hydrogel components, as well as to fabricate the corresponding fibro-gels.

Using this method to form the fibro-gel also yielded a high throughput with roughly 3 mL of fibro-gel (volume fraction = 50%) every 1 h operating a single channel device. The

ADVANCED MATERIALS

www.advmat.de

throughput can be increased significantly and easily using multiple streams.<sup>[17]</sup> This laboratory-scale experiment paves the way for the cost-effective and high-throughput fabrication of fibrogels at an industrial scale.

#### 2.2. Characterization of the Fibro-Gel

#### 2.2.1. Controllable Physicochemical Properties of Fibro-Gel

The micromorphology of the hydrogel was observed by scanning electron microscopy (SEM). The structures revealed that the fundamental process of gelation is mechanical, in which fibers flex (bend, twist, form loops, etc.) and form topological entanglements as a result of extrusion, as shown in Figure 1d.

By changing  $L_{\rm fiber}$  we were able to generate fibro-gels with distinct properties. The fibro-gels with the same fiber diameter (110  $\mu$ m) but different fiber lengths were formed with the same fiber volume fraction (50%) from a needle with the same extrusion rate. Individual confocal z-slices of fibro-gels created with different  $L_{\rm fiber}$  were taken (**Figure 2a**), showing a 3D structure formed by coiled fibers. With an increase of  $L_{\rm fiber}$  from 8.8 to 220 mm, the number of looped and coiled fibers increased, indicating that fibro-gels with longer fiber lengths had more complex topological entanglements. Based on the confocal images, the porosity of the fibro-gels for different  $L_{\rm fiber}$  was explored. As shown in Figure 2b, the porosity of the fibro-gel decreased with an increase in the fiber length, which was a direct consequence of more complex topological entanglements.

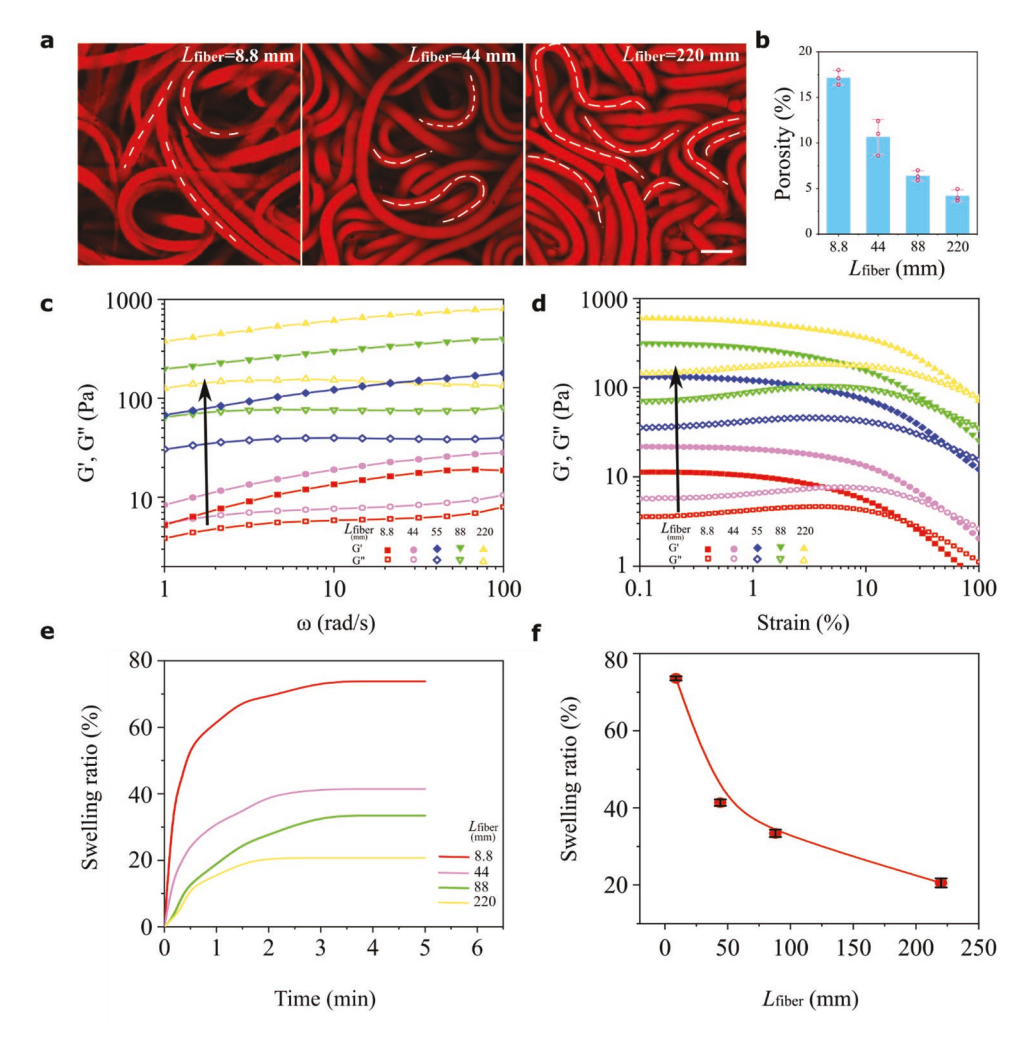


Figure 2. Characterizations of the fibro-gel. The properties of the fibro-gel, such as swelling ratio and modulus, depending on the length of the individual microfibers,  $L_{\rm fiber}$ . a) Individual confocal z-slices showing the microfiber deformations in the fibro-gels for different fiber lengths and the same fiber diameter produced with similar operating conditions. The number of looped and coiled fibers increases with  $L_{\rm fiber}$ . Scale bar: 200  $\mu$ m. b) The porosity of the fibro-gels for different fiber lengths decreases with the increase of  $L_{\rm fiber}$ . c) Frequency-sweep rheological properties of the fibro-gel for different fiber lengths. The elastic modulus G' (solid pattern) and viscous modulus G'' (hollow pattern) are measured using a parallel-plate rheometer. The fibro-gels exhibited an elastic-like behavior (i.e., G' > G''). Both G' and G'' increase with  $L_{\rm fiber}$ . The arrow highlights the increase for G' and G'' with increasing  $L_{\rm fiber}$ . d) Strain-sweep rheology study of fibro-gels for different fiber lengths. The arrow highlights the increase for G' and G'' with increasing  $L_{\rm fiber}$ . e,f) The tunable swelling behavior of the fibro-gels for different fiber lengths. The fibro-gels reached the equilibrium swollen state within 5 minutes. The fibro-gel with longer fiber lengths displayed a smaller swelling ratio.



www.advmat.de

To verify the mechanical properties of fibro-gels, rheological analysis as a function of frequency and strain were conducted using a parallel-plate rheometer.[15] To study the influence of L<sub>fiber</sub> on the mechanical properties of the fibro-gels, the rheological properties of the fibro-gels for different  $L_{\mathrm{fiber}}$  lengths were compared. As shown in Figure 2c,d, the fibro-gels exhibited an elastic-like behavior (i.e., G' > G'')<sup>[18]</sup> and both G' and G" increased with an increase in fiber length (indicated by the arrow); here G' indicates the elastic modulus and G'' indicates the viscous modulus. All the fibro-gels showed linear viscoelastic regions for strains < 10%; G' decreased at higher strain values due to the onset of network breakdown. Both the micro-network, which is the chemical crosslinking of the individual microfibers, and the macro-network, which is the entanglement among many microfibers, exist in the fibro-gels. With the same experimental conditions, the molecular scale, chemical crosslinking of the hydrogel should be the same. Hence, a qualitative explanation for the difference in the mechanical properties is that with an increase in the fiber length, the entanglements inside the fibro-gels become more complex with a larger number of looped and coiled fibers, which suggests that the main mechanism for the formation of the macro-network of the fibro-gels leads to the differences of G' and G''. These easily tunable mechanical properties allow the production of fibro-gels with a wide range of properties to be constructed for clinical use.

The fibro-gels also showed different swelling behaviors for different  $L_{\rm fiber}$  as shown in Figure 2e,f. The swelling ratio (%) of the fibro-gels was calculated as:

swelling ratio (%) = 
$$\frac{W_t - W_0}{W_0} \times 100\%$$
 (1)

where  $W_t$  was the weight of the swollen fibro-gel at time t and  $W_0$  was the weight of the initial fibro-gel before swelling. Although all of these fibro-gels reached an equilibrium swollen state within 5 min (Figure 2e), which illustrates the favorable swelling ability, the fibro-gel with longer fiber lengths displayed a smaller swelling ratio as shown in Figure 2f. Hydrogels with higher specific surface areas and larger pore sizes have larger swelling rates and lower swelling activation energies due to their faster response behavior. Thus, the measurements indicate that different fiber lengths would not only lead to different degrees of physical entanglements (Figure 2c,d), and so distinct rheological properties, but also to different surface areas and pore sizes of the fibro-gel.

# 2.2.2. Tunable Release Profile of Fibro-Gel

To explore the drug release profile of the fibro-gel, we first encapsulated tetracycline (TC) into the fibro-gels and measured the released amount of TC from the same volume of fibro-gels with different  $L_{\rm fiber}$  The cumulative drug release (%) and the drug release rate (mg per day) of the hydrogels were calculated as:

where  $P_t$  was the percentage released at time t and  $P_{t-\Lambda t}$  was the percentage released at the time of the previous measurement. As shown by the results in Figure 3a, fibro-gels with different fiber lengths have different drug release profiles. A fibro-gel with longer fibers provided a prolonged drug release time, which was calibrated by using a UV absorption spectrometer (see Experimental Section and Figure S1, Supporting Information). The drug release rates of fibro-gels with different  $L_{\rm fiber}$ showed that there was a rapid release rate (burst release) at earlier times as shown in Figure 3b (upper-right panel), which decreased with increasing fiber length, followed by a sustained release rate as shown in Figure 3b (bottom-right panel), which increased a small fraction with increasing fiber length. To demonstrate whether the fibro-gels can achieve tunable release of various cargo, the release rates of EGF from fibro-gels with different L<sub>fiber</sub> were explored in Figure 3c,d, showing that the EGF release profile changes with  $L_{\rm fiber}$  as well.

As part of the drug administration strategy, burst release has been used to deliver drugs at high release rates, [20] while sustained release can provide the ability to maintain a constant medication level within the body. [21] For instance, the drugs used at the beginning of wound treatment with an initial burst provide immediate relief followed by prolonged release to promote gradual healing. [2a] In accordance with the fiber-length-responsiveness, the fibro-gel could release the drug more rapidly when the fiber length is shorter and more slowly when the fiber length is increased (Figure 3b,d).

When a drug is incorporated into a swellable gel, the diffusivity of encapsulated molecules is directly affected by the degree of swelling and porosity of the gel.<sup>[22]</sup> The drug release kinetics is controlled by the increase in release area produced by the swelling phenomenon. The fibro-gel with shorter fibers has a faster response swelling behavior, higher swelling degree, and larger pore size (Figure 2a,b,e,f). Consequently, the drug is released faster from the fibro-gel with shorter fibers. Based on the fiber-length-dependent swelling property, the networks inside the fibro-gels were expected to be different, with the pore size inside the fibro-gel increasing with a decrease of fiber length; [22] thus, we have achieved on-demand, controlled delivery of therapeutics by using the fiber-length-dependent properties. For tissue engineering applications, different drugs (e.g., integrins, growth factors, and small molecule medicines) should be presented over different timescales during therapy so that coordinated cellular response can be accurately triggered. [2a,23] With the fiber-length-dependent drug release rate, we can achieve the controlled release of different drugs at different rates by loading drugs into different microfibers whose fiber lengths are different. An illustration of how this approach can be used on an actual wound is shown in Figure 3e. To confirm the assumption of the on-demand release of different drugs, 0.85 mg mL<sup>-1</sup> TC and 42.5 ng mL<sup>-1</sup> EGF were encapsulated into the 8.8 mm and 220 mm microfiber respectively to form a two-layer fibro-gel.

cumulative percentage release (%) = 
$$\frac{\text{Volume of sample withdrawn (mL)}}{\text{Bath volume (mL)}} \times P_{t-\Delta t} + P_t$$
 (2)

$$drug release rate (mg/day) = \frac{Cumulative drug release amount (mg)}{release time (day)}$$
(3)

15214095, 2023, 19, Downloaded from https://onlinelibrary.wiley.com/doi/10.1002/adma.202211637 by Princeton University, Wiley Online Library on [15/042024]. See the Terms and Conditions (https://onlinelibrary.wiley.com/ems

and-conditions) on Wiley Online Library for rules of use; OA articles are governed by the applicable Creative Commons License

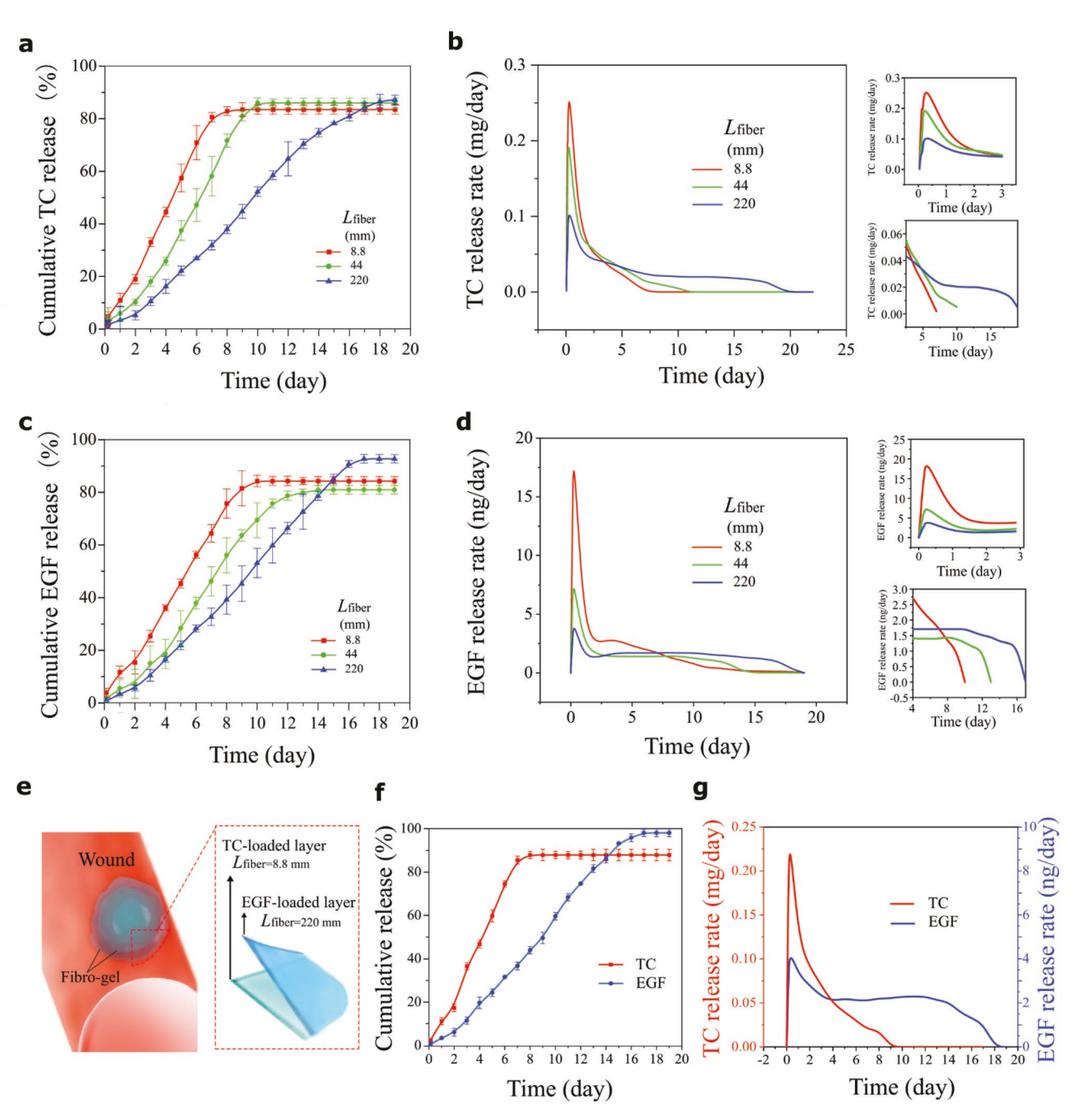


Figure 3. Drug release profile of the fibro-gel. The drug release rates of the fibro-gel can be adjusted by  $L_{\rm fiber}$ . a) The TC release profile of fibro-gels for different fiber lengths. The fibro-gel with longer fibers exhibits a more sustained drug release profile. Hydrolysis and/or the drug tightly entrapped in the gel also result in the incomplete release of the drug. b) The TC release rates of the fibro-gels for different fiber lengths show that there is a rapid release rate at earlier times (upper-right panel; burst release in the early stage), which decreases with increasing fiber length, followed by a sustained release rate (lower-right panel; sustained release in the later stage), which increases a small fraction with increasing fiber length. The drug release rates were calculated from the average cumulative drug release amount (Equation 3). c) The EGF release profile of fibro-gel for different fiber lengths. Hydrolysis and/or the drug tightly entrapped in the gel also result in the incomplete release of the drug. d) The EGF release rates of the fibro-gels for different fiber lengths show that there is a rapid release rate at earlier times (upper-right panel), which decreases with increasing fiber length, followed by a sustained release rate (lower-right panel), which increases a small fraction with increasing fiber length. e) Schematic illustration of a wound healing application of a two-layer fibro-gel encapsulating different drugs. The TC was loaded into the bottom layer with shorter fibers ( $L_{\text{fiber}} = 8.8 \text{mm}$ ), while the EGF was loaded in the upper layer with longer fiber ( $L_{\text{fiber}} = 220 \text{ mm}$ ). Two layers of the fibro-gel were extruded sequentially. f) The TC and EGF release profiles of the two-layer fibro-gel as shown in Figure 3e. The EGF that was loaded in the longer fibers has a prolonged release time compared with the TC loaded in the shorter fibers. g) The TC and EGF release rates of the two-layer fibro-gel. The TC in the shorter fibers has a rapid release rate. Release



www.advmat.de

The drug release profile and the drug release rates were measured as shown in Figure 3f,g. TC loaded into the shorter fiber layer has a shorter release time with a faster release rate, while EGF loaded into the longer fiber layer has a prolonged release time with a sustained release rate.

# 2.3. Biocompatibility Test

To assess the potential of the fibro-gel as a dressing for tissue engineering applications, in vitro cell culture experiments were carried out using a fibro-gel consisting of fibers of diameter 110  $\mu$ m and  $L_{\rm fiber}$  = 44 mm. Note that in the following in vitro and in vivo tests, for the fibro-gel with TC and EGF group (A), the TC and EGF were loaded together into the same fiber ( $L_{\rm fiber}$  = 44 mm). While for the fibro-gel with TC and EGF (different  $L_{\rm fiber}$ ) group (B), TC was loaded into the shorter fibers ( $L_{\rm fiber}$  = 8.8 mm), EGF was loaded into the longer fibers ( $L_{\rm fiber}$  = 220 mm), respectively. Afterward, two layers of the fibro-gel were extruded in sequence (see the schematic illustration in Figure 3e).

The biocompatibility of the fibro-gel was assessed using a Live/Dead assay and the Cell Counting Kit 8 (CCK8) during a 5-day culture of NIH 3T3 cells. In Figure 4a, fluorescence images of cell cytotoxicity testing for the control group, the commercial gel (Hydrosorb Gel) group, the fibro-gel without TC and EGF group, and the fibro-gel group with TC and EGF group (A) showed the condition of live cells (green) and dead cells (red) on days 1, 3, and 5. Over the course of the study, most cells retained their traditional spindle-like morphology, and on days 3 and 5 they still showed strong proliferative activity. Another control, cells treated with free EGF, was also performed (see Figure S4, Supporting Information), showing that the fibro-gel improves growth factor effectiveness over a simple bolus treatment. The mean optical density (OD, absorbance) was used to calculate the percentage of cell viability based on the quantitative results verified by the CCK-8 kit:

relative cell viability (%) = 
$$\frac{(OD_{\text{material}} - OD_{\text{DI water}})}{(OD_{\text{cell medium}} - OD_{\text{DI water}})} \times 100\%$$
 (4)

The cell viability values were plotted by averaging triplicate results. The relative cell viability values in all groups are shown in Figure 4b. For the first day, the cell viability in the fibro-gel with TC and EGF group was significantly higher than in the other three groups. Although there was no significant difference in the growth trend between control group and the fibrogel group with TC and EGF on the third day, by the fifth day it was clear that the cells were growing faster in the fibro-gel with TC and EGF group. The results of the fibro-gel without TC and EGF group also further demonstrated the favorable biocompatibility of the pure fibro-gel. All results confirmed that the NIH 3T3 cells used in this experiment maintained a classical spindle-like morphology throughout the experiment and had good viability and proliferation despite different concentrations of fibro-gels, which demonstrates the good biocompatibility of the fibro-gel (Figure 4c; Figure S2, Supporting Information).

The effects on cells of  $L_{\rm fiber}$  and fiber arrangement and orientation in the fibro-gels with different fiber lengths were also investigated (see Figure S3, Supporting Information). The

results showed that  $L_{\rm fiber}$  of fibro-gel did not affect the cell viability, as most of the cells still showed strong proliferative activity in the fibro-gel after 96 h, which demonstrates the good biocompatibility of the fibro-gel for different fiber lengths.

#### 2.4. Angiogenesis Assay in Vitro

Vasculogenesis is a major element in tissue engineering applications, [24] so tube-formation experiments were used to assess the effects of the fibro-gel on the angiogenesis process in vitro. In particular, the cell nucleus was stained by 4',6-diamidino-2-phenylindole (DAPI), and the actin filaments of the cells were stained by Phalloidin. The results in Figure 4d,e showed that the human umbilical vein endothelial cells (HUVECs) treated with the fibro-gel with TC and EGF (14.7  $\pm$  1.5 mm) or the fibro-gel without TC and EGF (11.1  $\pm$  0.3 mm) exhibited more junctions and longer tube lengths than the control group (1.5  $\pm$  0.5 mm) and the commercial gel group (Hydrosorb Gel) (7.3  $\pm$  1.3 mm). Another control, HUVECs treated with free EGF, has been conducted (see Figure S5, Supporting Information), indicating that the sustained delivery improves vascularization. Although vascular tube formation appeared in the control group and the commercial gel group, the tubular framework seemed less complete and with a smaller number of junctions and tube lengths compared to the fibro-gel group.

#### 2.5. In Vivo Proof-of-Concept of the Efficacy of the Fibro-Gel

The excisional wound healing model<sup>[25]</sup> is an animal model in which a small piece of full-thickness skin is completely removed from the wound bed. The assessment of epithelialization, granulation tissue formation, scar formation, and angiogenesis can be achieved in this single model. Thus, it is a good model for assessing the fibro-gel's in vivo biocompatibility and the potential of accelerating the repair of tissues,[26] Therefore, the tissue regeneration efficiency of the commercial gel, the fibro-gel without TC and EGF, and the fibro-gel with TC and EGF were investigated in vivo by a mice excision skin model as shown in Figure 5a. The healing results at various times are shown in Figure 5b. In the control group, dressings were not applied to the wounds while in the commercial gel group and the fibro-gel group, the mice were dressed, respectively, with corresponding hydrogels. In the free TC and EGF group, the mice were treated with 0.85 mg TC and 42.5 ng EGF on day 0. On day 4, a lot of yellow pus (indicated by the dashed line) was seen scattered in the wound bed in the control group indicating a wound infection, while it was rarely detected in the other groups over the course of the study. On the same day, compared with other groups, the wound healing area was minimized in the fibrogel with TC and EGF group (B) (different  $L_{\text{fiber}}$ ), indicating that infection had been managed effectively, the inflammation was significantly reduced, and the wound repair process accelerated wound healing at the early stage, which is an advantage of the faster release of TC from the first-layer fibro-gel, as shown in Figure 5c. The wound healing area in the control group expanded slowly in the first 8 days, which could mean that the infection was not under control. In contrast, in the

ditions) on Wiley Online Library for rules of use; OA articles are governed by the applicable Creative Commons License

www.advancedsciencenews.com

www.advmat.de

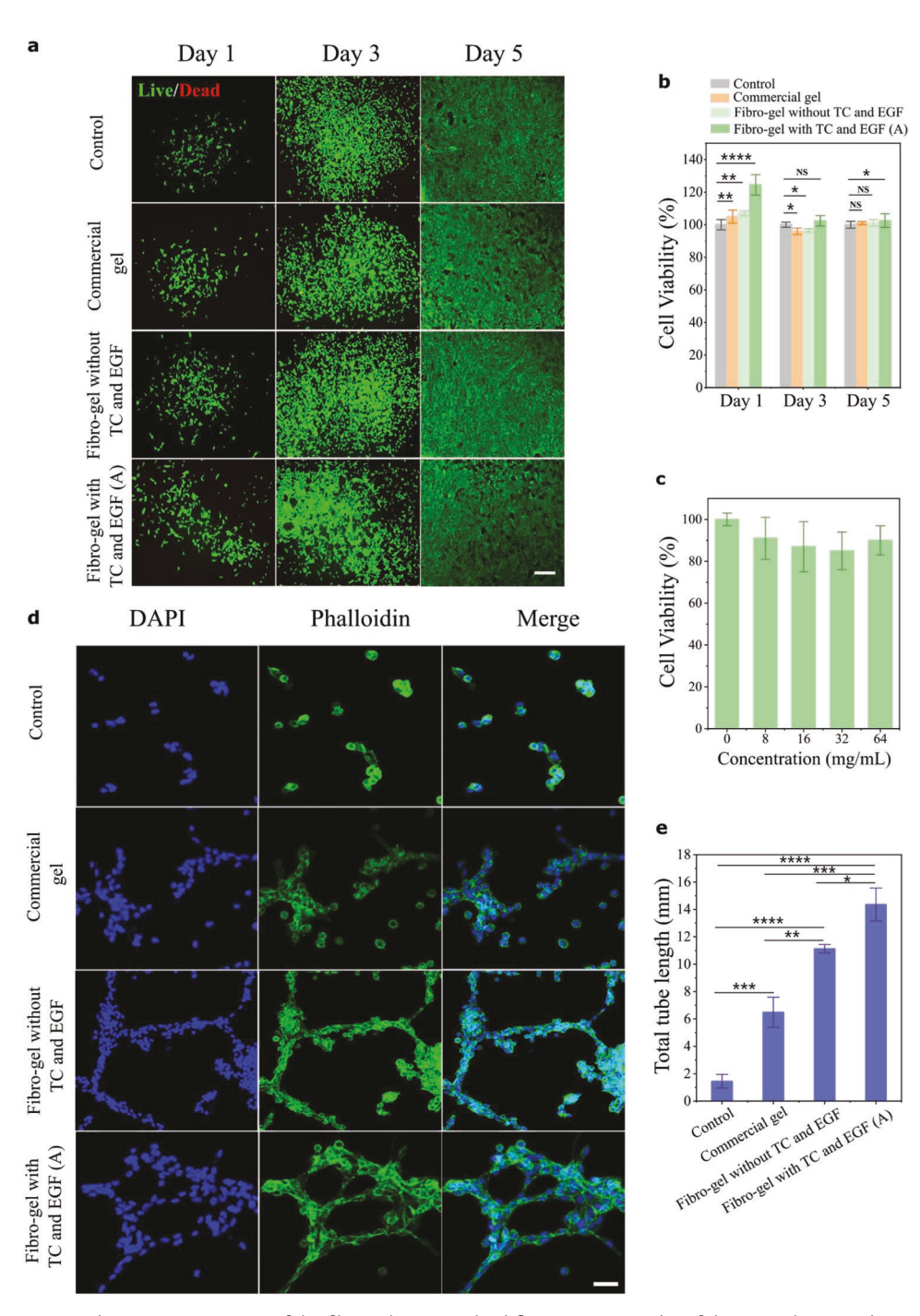


Figure 4. Cell cytotoxicity and angiogenesis assay of the fibro-gel. a) Live/dead fluorescence results of the control group, the commercial gel group (Hydrosorb Gel), the fibro-gel without TC and EGF group, and the fibro-gel with TC and EGF group (A). Fluorescence images of cell cytotoxicity testing for the four groups showing the condition of live cells (green) and dead cells (red) on days 1, 3, and 5. Scale bar:  $500 \, \mu m$ . b) Cell viability as determined with NIH 3T3 cell counting CCK-8 assay for the control group, the commercial gel group, and the fibro-gel group for 1, 3, and 5 days. The concentration of hydrogel is the same in each gel group at  $10 \, \text{mg mL}^{-1}$ . c) Cell viability using CCK-8 assay following treatment with different concentrations of fibro-gels with TC and EGF (A) for 24 h. d) Vascular tube-formation in vitro of HUVECs for the control group, the commercial gel group, and the fibro-gel group at 6 h. Scale bar:  $40 \, \mu m$ . e) The total vascular tube length for the control group, the commercial gel group, and the fibro-gel group at 6 h. (NS, not significant, \*p < 0.05, \*\*p < 0.01, \*\*\*p < 0.001, \*\*\*\*p < 0.0001).

fibro-gel with TC and EGF group (B) (different  $L_{\rm fiber}$ ), antibiotic (TC) release in the early stages effectively shortened the antiinflammatory time and accelerated wound healing into the later stages. The sustained release of EGF from the second layer also accelerated cell proliferation and remodeling. The healing rate on day 8 of the fibro-gel with TC and EGF group (B) (different  $L_{\text{fiber}}$ ) (98.3  $\pm$  0.7%) was higher than that of the control group (48.7  $\pm$  1.9%), the commercial gel group (61.8  $\pm$  2.5%), the free

15214095, 2023, 19, Downloaded from https://onlinelibrary.wiley.com/doi/10.1002/adma.202211637 by Princeton University, Wiley Online Library on [15/04/2024]. See the Terms and Conditions

ditions) on Wiley Online Library for rules of use; OA articles are governed by the applicable Creative Commons License

www.advmat.de

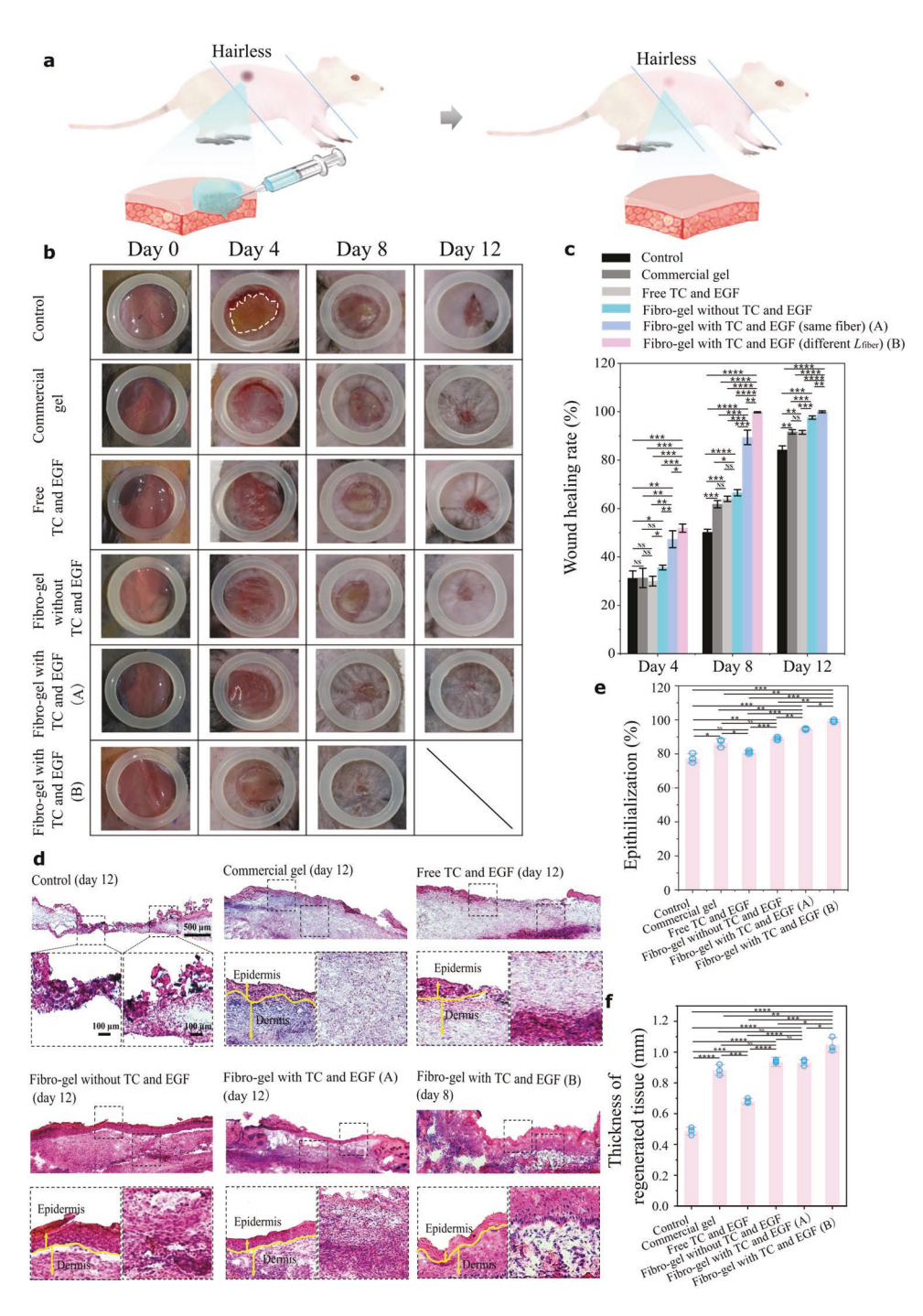


Figure 5. In vivo proof-of-concept of the efficacy of the fibro-gel. a) Schematic of the mice excision skin model. A full-thickness circle of skin with a 1 cm diameter was excised. In the control group, the mice were not dressed while in the commercial gel group (Hydrosorb Gel), the fibro-gel without TC and EGF group, the fibro-gel with TC and EGF group (A) (same  $L_{\text{fiber}}$ ), and the fibro-gel with TC and EGF group (B) (different  $L_{\text{fiber}}$ ), the mice were dressed with the commercial gel and the corresponding fibro-gel respectively. In the free TC and EGF group, the mice were treated with 0.85 mg TC and 42.5 ng EGF on day 0. b) Photographs of mice skin wound tissues for different groups on days 0, 4, 8, and 12, showing that the wound site of the fibro-gel group with TC and EGF in different fiber lengths is substantially reduced. The inner diameter of the rubber ring is 1 cm. c) Measured wound healing rate of different groups for 4, 8, and 12 days, showing the fastest wound healing rates occur with the fibro-gel with TC and EGF group (B). Hematoxylin and eosin (H&E) staining of skin tissue for the control group, the commercial gel group, the fibro-gel with TC and EGF group, the fibro-gel with TC and EGF group (B) on day 8. In the fibro-gel with TC and EGF group (B), the magnified images showed the complete epithelium and dermis structures, while in the control group, the free TC and EGF group, the fibro-gel with TC and EGF



www.advmat.de

TC and EGF group (63.2  $\pm$  1.5%), and the fibro-gel with TC and EGF group (A) (88.1  $\pm$  4.8%); these indicate a significant effect on promoting wound healing as shown in Figure 5b,c. When the treatment was extended, the healing area of the wound continued increasing, and a 98.3  $\pm$  0.7% wound closure rate was reached on day 8 in the fibro-gel with TC and EGF group (B) (different  $L_{\rm fiber}$ ) (Figure 5b,c), when compared with that in the free TC and EGF group (90.5 $\pm$  0.9%), the commercial gel group (91.7  $\pm$  1.0%), the fibro-gel with TC and EGF group (A) (95.8  $\pm$  1.3%) and the control group (82.5  $\pm$  3.2%) on day 12. As evidenced by the macroscopic observations, the fibro-gel exhibited significant potential to expedite the complex process of tissue regeneration, which required both antibacterial activity and vascularization.

# 2.6. Histological Analysis

#### 2.6.1. Hematoxylin and Eosin Staining

The wound samples at each time point were harvested and the frozen sections were utilized for hematoxylin and eosin (H&E) staining. As illustrated in Figure 5d, in the control group the regenerated skin tissue displayed the typical appearance of scar tissue with a flattened epidermis after 12 days of treatment. In the commercial gel group, the regenerated tissue displayed a similar appearance, but with a thicker overall tissue compared with the control group (Figure 5d,e). However, in the fibro-gel with TC and EGF group (B) (different  $L_{\text{fiber}}$ ), the defect was almost closed after 8 days of treatment and the regenerated skin tissue revealed a de novo regenerated appearance that almost has no difference from normal tissue (Figure 5d-f). Overall, there was poor epithelialization in both the control and commercial gel groups histologically, whereas the fibro-gel with TC and EGF group (B) (different  $L_{\text{fiber}}$ ) showed complete re-epithelialization after 8 days of treatment.

#### 2.6.2. Immunofluorescence Staining

Furthermore, we also used an immunofluorescence stain to determine if the potential to vascularize was present. The fluorescence expressions of vascular smooth muscle cells marker α-SMA and vascular endothelial-specific marker CD31 were tested as shown in Figure 6a,b. α-smooth muscle actin (α-SMA) is often used as a marker of myofibroblast formation and CD31 is a protein that in humans is encoded by the PECAM1 gene which can help to evaluate the degree of tissue angiogenesis. The corresponding results on day 12 for the control group, the commercial gel group, and the free TC and EGF group, shown in Figure 6c,d, revealed minimal α-SMA and CD31 expression during the whole period. Conversely, the fluorescence intensity of α-SMA and CD31 expression intensity in the fibro-gel

with TC and EGF group (B) (different  $L_{\rm fiber}$ ) on day 8 was 25.1  $\pm$  2.7 and 27.3  $\pm$  2.3 respectively, which were significantly higher than the expression intensity in the other groups. The higher expression of  $\alpha$ -SMA in the fibro-gel group also indicates more myofibroblast formation during the wound healing process. Myofibroblast can be derived from the transition of fibroblast through mechanical and physical regulation. The fibro-gel may have provided the physical stimuli. The faster wound healing or closure of the wound in the fibro-gel group may also be the result of the myofibroblast contraction. Overall, we conclude that the fibro-gel provided an excellent 3D sterile microenvironment platform for reconstructing a vascular network and was more effective for improving tissue regeneration based on all of the aforementioned findings.

# 3. Conclusion

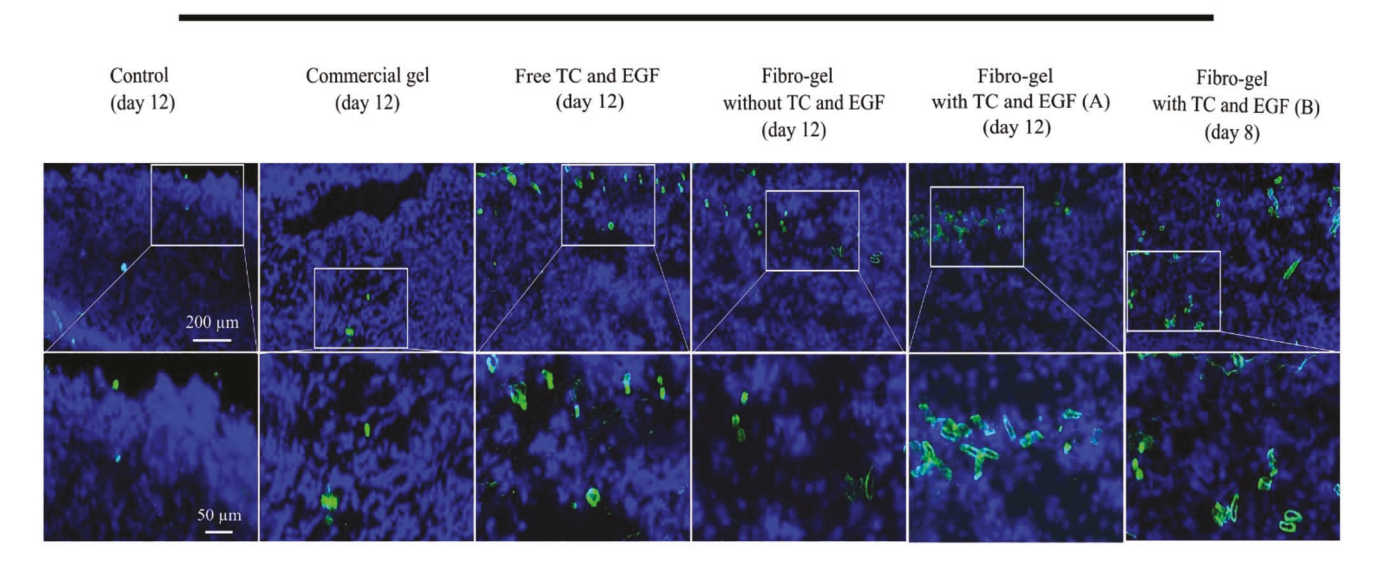
We have designed and fabricated an oil-free, biocompatible, biomimetic, and fully scalable fibro-gel for tissue engineering applications. A considerable range of physicochemical properties and drug release rates can be modulated for our fibro-gel by simply adjusting the microfiber lengths. Thus, fibro-gels have a wide range of properties that can be constructed for clinical use. Combining the tunable properties and the "plug and play" nature of this microfluidically generated strategy allows the incorporation of diverse already established materials (for example, fibrin or hyaluronic acid), signals (for example, growth factors), and cell populations (for example, stem cells). Complex combinations of microfibers with different fiber lengths with deterministic chemical and physical properties may enable tissue regeneration in a variety of distinct physiological niches (for example, neural, cardiac, skin, and so on). We also demonstrated, by using a mice excision skin model, that the fibro-gel has favorable biocompatibility and accelerated tissue regeneration ability. The preliminary in vivo test results showed the considerable advantages of the fibro-gel with a faster new tissue regeneration rate and healthier de novo regenerated tissue when compared with the commercial gel. In the future, we need to further evaluate the tunable properties and the effects of complex combinations of microfibers with different drugs or cells in different animal models. Overall, the unique combination of scalable, injectable, and tunable physicochemical properties of fibro-gel has the potential to introduce a new approach toward a precisely tailored gel for in situ tissue engineering.

# 4. Experimental Section

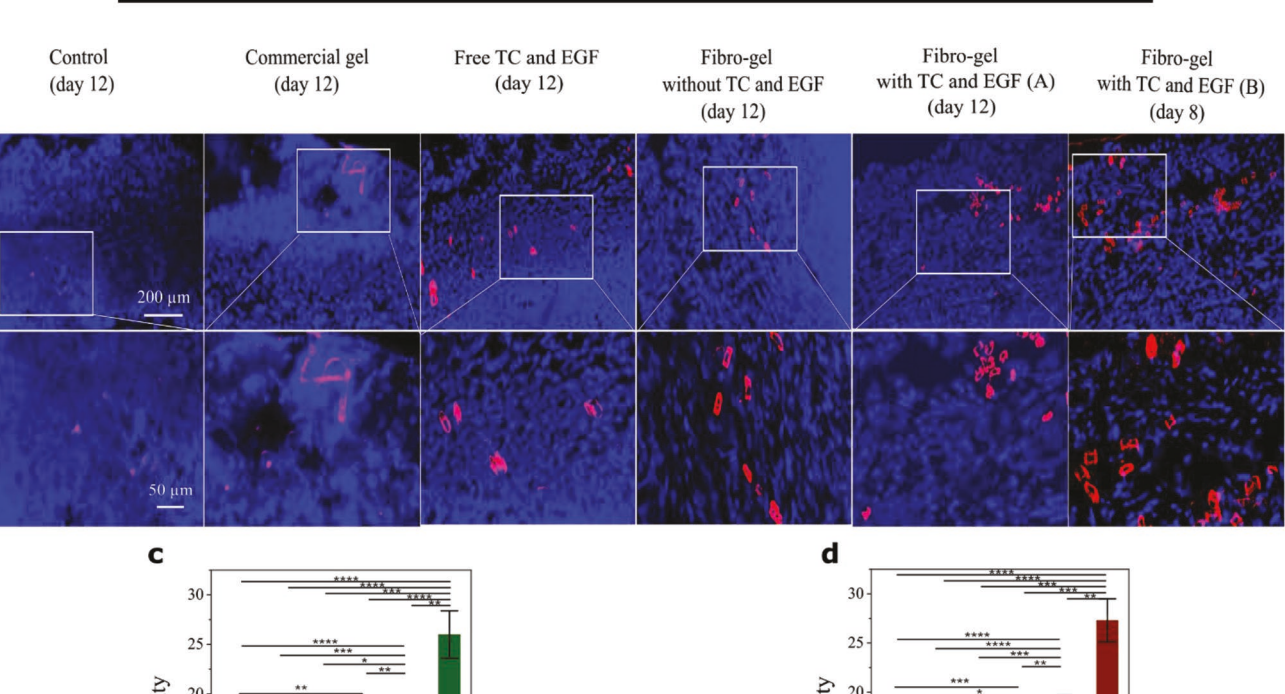
Fabrication of the Fibro-Gel: Microfibers were made by an aqueous two-phase system (ATPS), poly(ethylene glycol) diacrylate (PEGDA, Mw = 575 g mol<sup>-1</sup>, 25 wt.%; Sigma), and potassium phosphate tribasic (6 wt%; Sigma). The polymer-rich phase was mixed with 1 wt.% of the photo-initiator, lithium phenyl-2,4,6-trimethylbenzoylphosphinate (LAP; Sigma),

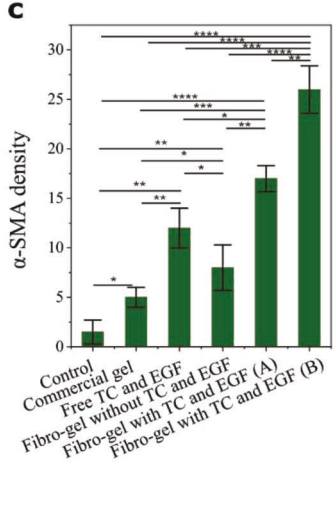
a

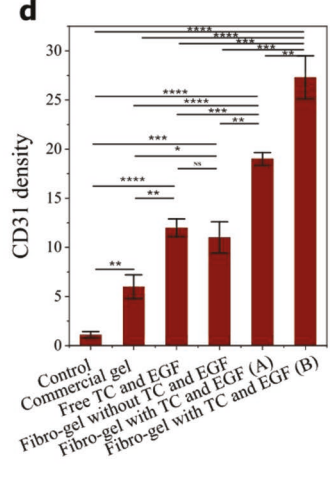
α-SMA/DAPI



# b CD-31/DAPI









www.advmat.de

and the drugs, 1 mg mL<sup>-1</sup> tetracycline (TC; Sigma) and/or 50 ng mL<sup>-1</sup> epidermal growth factor (EGF; Thermo Fisher); this solution was used as the inner phase of the co-flow. Pulsed UV illumination was used to polymerize the aqueous jet into uniform microfibers. By tuning the UV curing time, the length of the microfiber can be changed.

After collecting a certain volume of microfiber, the microfibers were washed three times with DI water. Then the drug-loaded microfiber suspension (fiber volume fraction = 50%) was extruded from a standard needle (0.5" long 27 G needle, inner diameter = 0.21 mm) at a constant extrusion rate 65 mL  $h^{-1}$  by syringe pump to form a fibro-gel. The concentrations of the TC and EGF in the fibro-gel after washing were calibrated at 0.85 mg mL $^{-1}$  and 42.5 ng mL $^{-1}$ .

Characterization of the Fibro-Gel: Scanning electron microscopy: Freeze-dried fibro-gel was adhered on an aluminum substrate using carbon tape and coated with a small amount of gold for 30 s. The coated samples were observed by SEM (HITACHI S-4800).

Confocal z-slices were performed on a laser-scanning confocal microscope (Zeiss). Fluorescent dye, rhodamine 6G (sigma), was used for imaging.

Rheological Measurements: The rheological properties of the fibro-gel were measured using a stress-controlled rheometer. [15] All experiments were carried out at room temperature (23 °C). To minimize the effect of wall slip, we used a rough parallel plate with a diameter of 50 mm. The measurement gap was fixed at 1 mm, and the shear stress was set at a constant 0.7 Pa.

Drug Release Profile: The released amount of tetracycline (TC) and/ or epidermal growth factor (EGF) from the fibro-gels for different fiber lengths was detected in PBS (pH = 7.4). The fibro-gels (1 mL) were immersed in 15 mL of PBS and the samples were shaken at 25 rpm on a rotary shaker at 37 °C throughout the release study.<sup>[27]</sup> At certain time intervals ( $\Delta t = 1, 2, 3, 4, 5,10$  h, and every 24 h), 1 mL of the solution was removed for measurement and an equal volume of fresh PBS was added. UV-vis spectrophotometer (Shimadzu) was used to measure the amount of released TC. The released amount of EGF in the collected PBS solution was quantified using an EGF ELISA kit (Thermo Fisher). For the two-layer fibro-gel, the TC-loaded layer was extruded from the shorter fiber suspensions ( $L_{fiber} = 8.8 \text{ mm}$ ; 1 mL) followed by extruding the second layer of EGF-loaded fibro-gel ( $L_{\text{fiber}} = 220 \text{ mm}$ ; 1 mL) on the top of the first layer. Due to the high viscosity of the fibro-gel itself, there was no additional reaction between the two layers. The two-layer fibro-gels were immersed in 15 mL of PBS and the samples were shaken at 25 rpm on a rotary shaker at 37 °C throughout the release study. At certain time intervals ( $\Delta t = 1$ , 2, 3, 4, 5,10 h, and every 24 h), release experiments were conducted in triplicate and results were presented as the average  $\pm$  standard deviation. The cumulative drug release (%) and the drug release rates of the TC and/ or EGF were calculated according to Equations 2 and 3.

Cell Experiments: NIH 3T3 and HUVEC cells (Thermo Fisher) were used for in vitro experiments. The cells were incubated in DMEM (Gibco) supplemented with 10% fetal bovine serum (Gibco), 1% penicillin-streptomycin solution (Hyclone) and incubated in a  $CO_2$  constant temperature incubator.

Biocompatibility Test: NIH 3T3 cells were seeded in 96-well plates at proper density and cultured with the DMEM buffer in the control group, with 10 mg mL<sup>-1</sup> commercial hydrogel in the commercial group, and with 10 mg mL<sup>-1</sup> microfiber-based hydrogel in the fibro-gel group. After 1, 3, and 5 days of incubation, CCK-8 reagent (Dojindo) was mixed with fresh DMEM medium for culturing for 4 h and cell viability was quantified by a microplate reader at 450 nm (Molecular Devices). Additionally, the Live/Dead kit (Invitrogen) was comprised of calcein-AM (green fluorescence) and ethidium homodimer-1 (red fluorescence) that were employed to assess NIH 3T3 cell viability. The fluorescent images were acquired using a Nikon Ti2-E Widefield microscope. Also, different concentrations (0, 8, 16, 32, and 64 mg mL<sup>-1</sup>) of fibro-gels were cultured with the NIH 3T3 cells for 24 h to verify the cell viability.

Angiogenesis Assay In Vitro: Growth factor-reduced basement membrane extract Matrigel (200 µL; Corning) was used as a culture substratum. A thin layer (10 µL per well) of commercial gel, fibro-gel without TC and EGF, fibro-gel with TC and EGF (A) were laid over the prechilled 24-well culture plates in the commercial gel group, the fibro-gel without TC and EGF group, and the fibro-gel with TC and EGF group (A) respectively. The concentrations of the TC and EGF in the fibro-gel with TC and EGF group (A) were 0.85 mg  $\,\mathrm{mL^{-1}}$  and 42.5 ng mL<sup>-1</sup>. The free EGF group was added with 42.5 ng mL<sup>-1</sup> EGF while the control group received nothing (all in triplicate). HUVEC cells were seeded in the prepared 24-well plates at proper densities and cultured in a CO<sub>2</sub> constant temperature incubator. The morphology was monitored under the optical microscope regularly. After 6 h, the wells were rinsed with PBS three times and then fixed with 4% polyformaldehyde (PFA; Sangon Biotech), permeabilized with 0.2% Triton X-100 (Sigma), and stained with phalloidin (Invitrogen) and DAPI (Sigma) solution. Fluorescence images were acquired using a laser scanning confocal microscope (Zeiss), and vascular tube lengths were quantified by Image J Software in five randomly selected fields of view.

Animal Tests: The animal experiments were carried out according to a protocol approved by the Committee on the Use of Live Animals in Teaching and Research (CULATR, the University of Hong Kong: 5805-21), which adheres to The International Guiding Principles for Biomedical Research Involving Animals and The Hong Kong Code of Practice for Care and Use of Animals for Experimental Purposes. In total, 36 male, 8-week-old C57BL/6N mice weighing ≈20 grams were used in the experiment (The University of Hong Kong; CULATR no. 5805-21). The mice were separated into six groups (the control group, commercial gel group, free TC and EGF group, fibro-gel without drug TC and EGF group, fibro-gel with TC and EGF (same  $L_{fiber}$ ) group (A), and fibro-gel with TC and EGF (different  $L_{fiber}$ ) group (B) (see Figure 5) for 4 different days (day = 0, 4, 8, and 12; n = 3for each timepoint for each group). Two circles with 1.0 cm diameter fullthickness skin were excised on the back of mice. The control group and the fibro-gel with TC and EGF group (A) were tested by the same mice for 12 days. The commercial gel group and the fibro-gel without TC and EGF group were tested by the same mice for 12 days. The free TC and EGF group and the fibro-gel with TC and EGF group (B) were tested by the same mice for 12 days. Anesthesia is achieved with an intraperitoneal injection of pentobarbital sodium solution at a dose of 50 mg kg<sup>-1</sup>. In the control group, the mice were not dressed, while in the commercial gel group, the fibro-gel without TC and EGF group, and the fibro-gel with TC and EGF group (A and B), the mice were dressed in the corresponding hydrogel with the same volume (1 mL) respectively. In the free TC and EGF group and the fibro-gel with TC and EGF group (A and B), the concentrations of TC and EGF were 0.85 mg mL<sup>-1</sup> and 42.5 ng mL<sup>-1</sup> respectively.

In Vivo Wound Healing: The criteria of complete healing of the wound were defined by the denuded wound being completely covered by layers of keratinocytes, and a newly stratified epidermis with underlying basal lamina re-established from the margins of the wound. The skins in various groups were harvested immediately after the wounds healed completely. H&E trichrome stain and immunohistochemical test were carried out in each group. The closure rate of the wound in different groups at each time point was calculated by the formula: healing rate (%) =  $(A_0[\text{initial wound area}] - A_t$  [residual wound area at each time point])  $/(A_0[\text{initial wound area}]) \times 100\%$ .

Histological Analysis: The wound samples at each time point were harvested and the frozen sections were utilized for hematoxylin and eosin (H&E) staining. The epithelialization of the control group, the commercial gel group, the free TC and EGF group, the fibro-gel without TC and EGF group, and the fibro-gel with TC and EGF group (A) on day 12 were calculated. While the epithelialization of the fibro-gel with TC and EGF group (B) on day 8 was calculated. The percentage

Figure 6. Immunofluorescence staining of α-SMA and CD31 for different groups. a,b) Histological section images of mice skin wound tissues with immunohistochemistry staining of protein α-SMA (green) and CD31(red) for the control group, the commercial gel group, the free TC and EGF group, the fibro-gel without TC and EGF group, the fibro-gel with TC and EGF group (A) on day 12 and the fibro-gel with TC and EGF group (B) on day 8. Scale bars are 200 μm in the top row and 50 μm in the bottom row. c) Measured α-SMA density in (a) for different groups (n = 3). d) Measured CD31 density in (b) for different groups. (n = 3; NS, not significant, \*p < 0.05, \*\*p < 0.01, \*\*\*\*p < 0.001, \*\*\*\*p < 0.0001).



www.advmat.de

of epithelialization was calculated based on the H&E staining images according to the equation: 1 – (pixels open wound area/pixels total wound area)  $\times$  100%. Means of epithelialization were calculated based on 15–20 random site measurements. Immunofluorescence, such as  $\alpha$ -SMA (Abcam) and CD31 (Abcam), was used to analyze collagen deposition and angiogenesis. All images were captured using a fluorescence microscope (Zeiss).

Statistical Analyses: All experiments were repeated at least three times. The data were analyzed by one-way ANOVA followed by Tukey's test (GraphPad Prism software) where p < 0.05 meant a significant difference. (NS, not significant, \*p < 0.05, \*\*\*p < 0.01, \*\*\*\*p < 0.001, \*\*\*\*p < 0.0001.)

# **Supporting Information**

Supporting Information is available from the Wiley Online Library or from the author.

# Acknowledgements

This project is supported by Research Grant Council of Hong Kong through the Research Impact Fund (No. R7072-18), with H.C.S. as the Project Coordinator, and J.K.N., H.A.S., and M.K.T.T. as co-principal-investigators under a collaborative project. This research is partially supported by the Health@InnoHK program of the Innovation and Technology Commission of the Hong Kong SAR Government as well as by NSF through the Princeton University (PCCM) Materials Research Science and Enigneering Center DMR-2011750. The authors thank Aviva S.F. Chow, Qingchuan Li, and Yi Pan for careful reading of the manuscript and their critical feedback. The authors also thank Jiaying Liu and Sihan Liu for their help with the cell experiment.

# **Conflict of Interest**

H.C.S. is a scientific advisor of EN Technology Limited, and MicroDiagnostics Limited, in both of which he owns some equity, and also a managing director of the research center, namely Advanced Biomedical Instrumentation Centre Limited. The works in the paper are however not directly related to the works of these two entities, as far as the authors know. The other authors declare no conflict of interest.

# **Author Contributions**

Y.S. and Y.L. contributed equally to this work. Y.S. and Y.L. designed research; Y.S. and Y.L. performed research; Y.S., Y.L., J.K.N., M.K.T.T., H.A.S., and H.C.S. analyzed data; Y.S., Y.L., J.K.N., H.A.S., and H.C.S. wrote the paper and all authors commented on the paper.

# **Data Availability Statement**

The data that support the findings of this study are available from the corresponding author upon reasonable request.

# Keywords

biomaterials, drug deliveries, injectable hydrogels, microfluidics, wound healing

Received: December 12, 2022 Revised: February 6, 2023 Published online: March 24, 2023

- [1] a) Z. Wang, H. Cui, M. Liu, S. L. Grage, M. Hoffmann, E. Sedghamiz, W. Wenzel, P. A. Levkin, Adv. Mater. 2022, 34, 2107791; b) F. M. Yavitt, T. E. Brown, E. A. Hushka, M. E. Brown, N. Gjorevski, P. J. Dempsey, M. P. Lutolf, K. S. Anseth, Adv. Mater. 2020, 32, 1905366; c) T. Yu, L. Zhang, X. Dou, R. Bai, H. Wang, J. Deng, Y. Zhang, Q. Sun, Q. Li, X. Wang, B. Han, Adv. Sci. (Weinh). 2022, 9, 2203734.
- [2] a) J. Li, D. J. Mooney, *Nat. Rev. Mater.* 2016, 1, 16071; b) G. Kiaee,
   P. Mostafalu, M. Samandari, S. Sonkusale, *Adv. Healthcare Mater.* 2018, 7, 1800396.
- [3] a) Y. S. Zhang, A. Khademhosseini, Science 2017, 356, 6337;
   b) D. R. Griffin, W. M. Weaver, P. O. Scumpia, D. Di Carlo, T. Segura, Nat. Mater. 2015, 14, 737.
- [4] a) Z. Tu, Y. Zhong, H. Hu, D. Shao, R. Haag, M. Schirner, J. Lee, B. Sullenger, K. W. Leong, Nat. Rev. Mater. 2022, 7, 557; b) Y. Liu, J. Liu, S. Chen, T. Lei, Y. Kim, S. Niu, H. Wang, X. Wang, A. M. Foudeh, J. B. Tok, Z. Bao, Nat. Biomed. Eng. 2019, 3 58
- [5] Y. Wang, L. Li, Y. Ma, Y. Tang, Y. Zhao, Z. Li, W. Pu, B. Huang, X. Wen, X. Cao, J. Chen, W. Chen, Y. Zhou, J. Zhang, ACS Nano 2020, 14, 8202.
- [6] P. S. Briquez, L. E. Clegg, M. M. Martino, F. M. Gabhann, J. A. Hubbell, *Nat. Rev. Mater.* 2016, 1, 1.
- [7] L. J. Macdougall, T. E. Hoffman, B. E. Kirkpatrick, B. D. Fairbanks, C. N. Bowman, S. L. Spencer, K. S. Anseth, Adv. Mater. 2022, 34, 2202882.
- [8] X. Hao, T. Du, H. He, F. Yang, Y. Wang, G. Liu, Y. Wang, Adv. Mater. Interfaces 2022, 9, 2102184.
- [9] a) J. Kim, D. M. Francis, L. F. Sestito, P. A. Archer, M. P. Manspeaker, M. J. O'Melia, S. N. Thomas, *Nat. Commun.* 2022, *13*, 1479; b) X. Li, Y. Shou, A. Tay, *Adv Nanobiomed Res* 2021, *1*, 2000073.
- [10] C. C. Huang, S. Ravindran, Z. Yin, A. George, Biomaterials 2014, 35, 5316.
- [11] a) H. D. Lu, D. E. Soranno, C. B. Rodell, I. L. Kim, J. A. Burdick, Adv. Healthcare Mater. 2013, 2, 1028; b) K. Lee, J. A. Hubbell, Curr. Opin. Biotechnol. 2013, 24, 827.
- [12] a) L. Yu, J. Ding, Chem. Soc. Rev. 2008, 37, 1473; b) E. A. Appel, M. W. Tibbitt, M. J. Webber, B. A. Mattix, O. Veiseh, R. Langer, Nat. Commun. 2015, 6, 6295.
- [13] A. C. Yu, H. Chen, D. Chan, G. Agmon, L. M. Stapleton, A. M. Sevit, M. W. Tibbitt, J. D. Acosta, T. Zhang, P. W. Franzia, R. Langer, E. A. Appel, *Proc Natl Acad Sci* 2016, 113, 14255.
- [14] a) T. R. Cox, J. T. Erler, Dis Model Mech 2011, 4, 165; b) D. T. Butcher, T. Alliston, V. M. Weaver, Nat. Rev. Cancer 2009, 9, 108.
- [15] A. Perazzo, J. K. Nunes, S. Guido, H. A. Stone, Proc. Natl. Acad. Sci. 2017, 114, E8557.
- [16] a) GY. Chao, H. C. Shum, Chem. Soc. Rev. 2020, 49, 114; b) H. Y. Lo, Y. Liu, S. Y. Mak, Z. Xu, Y. Chao, K. J. Li, H. C. Shum, L. Xu, Phys. Rev. Lett. 2019, 123, 134501.
- [17] a) M. B. Romanowsky, A. R. Abate, A. Rotem, C. Holtze, D. A. Weitz, Lab Chip 2012, 12, 802; b) J. Kim, M. Hegde, S. H. Kim, T. K. Wood, A. Jayaraman, Lab Chip 2012, 12, 1157.
- [18] J. Yu, K. Wang, C. Fan, X. Zhao, J. Gao, W. Jing, X. Zhang, J. Li, Y. Li, J. Yang, W. Liu, Adv. Mater. 2021, 33, 2008395.
- [19] a) R. Censi, W. Schuurman, J. Malda, G. di Dato, P. E. Burgisser, W. J. A. Dhert, C. F. van Nostrum, P. di Martino, T. Vermonden, W. E. Hennink, Adv. Funct. Mater. 2011, 21, 1833; b) Y. Huang, M. Zeng, J. Ren, J. Wang, L. Fan, Q. Xu, Colloids Surf. A 2012, 401, 97.
- [20] a) X. Huang, C. S. Brazel, J. Control Release 2001, 73, 121;
  b) S. R. Benhabbour, M. Kovarova, C. Jones, D. J. Copeland, R. Shrivastava, M. D. Swanson, C. Sykes, P. T. Ho, M. L. Cottrell, A. Sridharan, S. M. Fix, O. Thayer, J. M. Long, D. J. Hazuda, P. A. Dayton, R. J. Mumper, A. D. M. Kashuba, J. V. Garcia, Nat. Commun. 2019, 10, 4324.





www.advmat.de

- [21] a) Y. Wang, X. Yang, X. Chen, X. Wang, Y. Wang, H. Wang, Z. Chen,
  D. Cao, L. Yu, J. Ding, Adv. Funct. Mater. 2022, 32, 2206554;
  b) Y. Lvov, W. Wang, L. Zhang, R. Fakhrullin, Adv. Mater. 2016, 28, 1227.
- [22] K. J. De France, F. Xu, T. Hoare, Adv. Healthcare Mater. 2018, 7, 1800396.
- [23] K. J. Rambhia, P. X. Ma, J Control Release 2015, 219, 119.
- [24] a) J. Vajda, M. Milojevic, U. Maver, B. Vihar, Biomedicines 2021, 9, 589; b) F. Simunovic, G. Finkenzeller, Cells 2021, 10, 1749.
- [25] L. Chen, R. Mirza, Y. Kwon, L. A. DiPietro, T. J. Koh, Wound Repair Regen 2015, 23, 874.
- [26] a) J. E. Neil, M. B. Brown, A. C. Williams, Sci. Rep. 2020, 10, 21192;
  b) A. L. Clement, G. D. Pins, Wound Heal. Biomater. Woodhead Publishing, 2016, pp. 253–275.
- [27] a) J. Koo, S. B. Kim, Y. S. Choi, Z. Xie, A. J. Bandodka, J. Khalifeh, Y. Yan, H. Kim, M. K. Pezhouh, K. Doty, G. Lee, Y.-Y. Chen, S. M. Lee, D. D'Andrea, K. Jung, K. Lee, K. Li, S. Jo, H. Wang, J.-H. Kim, J. Kim, S.-G. Choi, W. J. Jang, Y. S. Oh, I. Park, S. S. Kwak, J.-H. Park, D. Hong, X. Feng, C.-H. Lee, et al., Sci Adv. 2020, 6, eabb1093; b) K. Hirota, A. C. Doty, R. Ackermann, J. Zhou, K. F. Olsen, M. R. Feng, Y. Wang, S. Choi, W. Qu, A. S. Schwendeman, S. P. Schwendeman, J Control Release 2016, 244, 302.